ARTICLES
https://doi.org/10.1038/s41557-020-0506-4

nature chemistry

Single-molecule visualization of DNA G-quadruplex formation in live cells

Marco Di Antonio[1,2,7], Aleks Ponjavic[1,3,4,7], Antanas Radzevičius[1,7], Rohan T. Ranasinghe[1], Marco Catalano[1], Xiaoyun Zhang[1], Jiazhen Shen[5], Lisa-Maria Needham[1], Steven F. Lee[1], David Klenerman[1]✉ and Shankar Balasubramanian[1,5,6]✉

Substantial evidence now exists to support that formation of DNA G-quadruplexes (G4s) is coupled to altered gene expression. However, approaches that allow us to probe G4s in living cells without perturbing their folding dynamics are required to understand their biological roles in greater detail. Herein, we report a G4-specific fluorescent probe (SiR-PyPDS) that enables single-molecule and real-time detection of individual G4 structures in living cells. Live-cell single-molecule fluorescence imaging of G4s was carried out under conditions that use low concentrations of SiR-PyPDS (20 nM) to provide informative measurements representative of the population of G4s in living cells, without globally perturbing G4 formation and dynamics. Single-molecule fluorescence imaging and time-dependent chemical trapping of unfolded G4s in living cells reveal that G4s fluctuate between folded and unfolded states. We also demonstrate that G4 formation in live cells is cell-cycle-dependent and disrupted by chemical inhibition of transcription and replication. Our observations provide robust evidence in support of dynamic G4 formation in living cells.

G-quadruplexes (G4s) are non-canonical structures that can form within guanine-rich nucleic-acid sequences (Fig. 1a)[1,2]. Sequencing of G4s in human genomic DNA (G4-Seq) has revealed over 700,000 distinct sites that can form G4s, with notable G4 enrichment within gene promoters and at loci commonly amplified in cancers[3]. G4 structures have also been imaged ex vivo by immunofluorescence with G4-selective antibodies, both in fixed ciliates[4] and, more recently, in fixed human cells[5]. The G4-selective antibody BG4 has been used in chromatin immunoprecipitation followed by sequencing (ChIP-Seq), showing that just ~1% of the G4s identified in purified DNA by G4-Seq could be detected within chromatin[6]. ChIP-Seq experiments rely on measurements integrated over millions of cells and therefore provide only an average view of G4 incidence at given genomic loci. However, G4 homeostasis in cells is likely to be regulated by proteins, such as helicases, so ex vivo techniques that provide a snapshot of G4 distribution may hide important dynamic processes that can only be observed by live-cell imaging. Fluorogenic G4-binding probes for the detection of both RNA[7,8] and DNA[9,10] G4s in living cells have been reported. Generally, such probes are used at relatively high (μM) concentrations, which can result in global induction of G4 structures, perturbation of endogenous G4-folding dynamics and cellular stress/toxicity through binding to G4s globally. Furthermore, some observational approaches require environmentally responsive probes, which can pose limits on the quantitative study of specific G4 formation and complicate the disentangling of genuine G4 binding from environmental effects. We have pursued single-molecule fluorescence imaging of G4s in living cells to detect individual G4s in the nucleus of live cells at low nanomolar concentrations of fluorescent probe. The use of a G4-specific probe (SiR-PyPDS (**1**)) and a control probe (SiR-iPyPDS (**2**)), with poor affinity to G4s, together with ligand competition experiments, confirmed the specificity of G4s. Relatively low probe concentrations (nM) help avoid the global induction of G4s inherent in ensemble fluorescence methods. Specifically, only a small fraction (~4%) of G4s are bound by the probe, thus minimising the effect of the probe on global G4-folding dynamics. Herein, we report the detection of individual G4s in the nucleus of living human cells by single-molecule fluorescence imaging.

SiR-PyPDS (**1**) (Fig. 1b) was prepared by tethering the far-red fluorophore silicon-rhodamine (SiR)[11] to an analogue of an established G4 ligand, pyridostatin[12] (PyPDS), using linkers of different lengths (Extended Data Fig. 1). On binding to G4-folded oligonucleotides, all SiR-PyPDS analogues (**1**, **3** and **4**) (Supplementary Fig. 1) displayed a modest fluorescence increase (approximately fourfold), which is insufficient to confidently discriminate bound versus unbound probes in cells, but enabled evaluation of optimal linker length by fluorescence titrations. Binding titrations revealed the six carbon linker of SiR-PyPDS (**1**) (Fig. 1b) as being optimal for G4-binding selectivity of the PyPDS scaffold, displaying good binding towards MYC, c-KIT1 and h-TELO G4s with K_d values of 0.63 ± 0.08 μM, 1.0 ± 0.1 μM and 2.0 ± 0.8 μM, respectively, and no detectable binding to double- or single-stranded DNA (dsDNA or ssDNA; Supplementary Fig. 2). SiR-PyPDS (**1**) exhibited a quantum yield of 0.05 in solution that increases to 0.2 when the molecule is bound to MYC G4 (see Methods). We also designed and synthesized a novel PyPDS isomer (SiR-iPyPDS (**2**), Fig. 1b) that could act as a poor G4-binding control in live-cell experiments to support unambiguous identification of G4-binding events by SiR-PyPDS. Our control analogue SiR-iPyPDS (**2**) differs from SiR-PyPDS (**1**) simply in the position of the amino side chains on the quinoline ring.

[1]Department of Chemistry, University of Cambridge, Cambridge, UK. [2]Imperial College London, Chemistry Department, Molecular Science Research Hub, London, UK. [3]School of Physics and Astronomy, University of Leeds, Leeds, UK. [4]School of Food Science and Nutrition, University of Leeds, Leeds, UK. [5]Cancer Research UK, Cambridge Research Institute, Li Ka Shing Centre, Cambridge, UK. [6]School of Clinical Medicine, University of Cambridge, Cambridge, UK. [7]These authors contributed equally: Marco Di Antonio, Aleks Ponjavic, Antanas Radzevičius. ✉e-mail: dk10012@cam.ac.uk; sb10031@cam.ac.uk

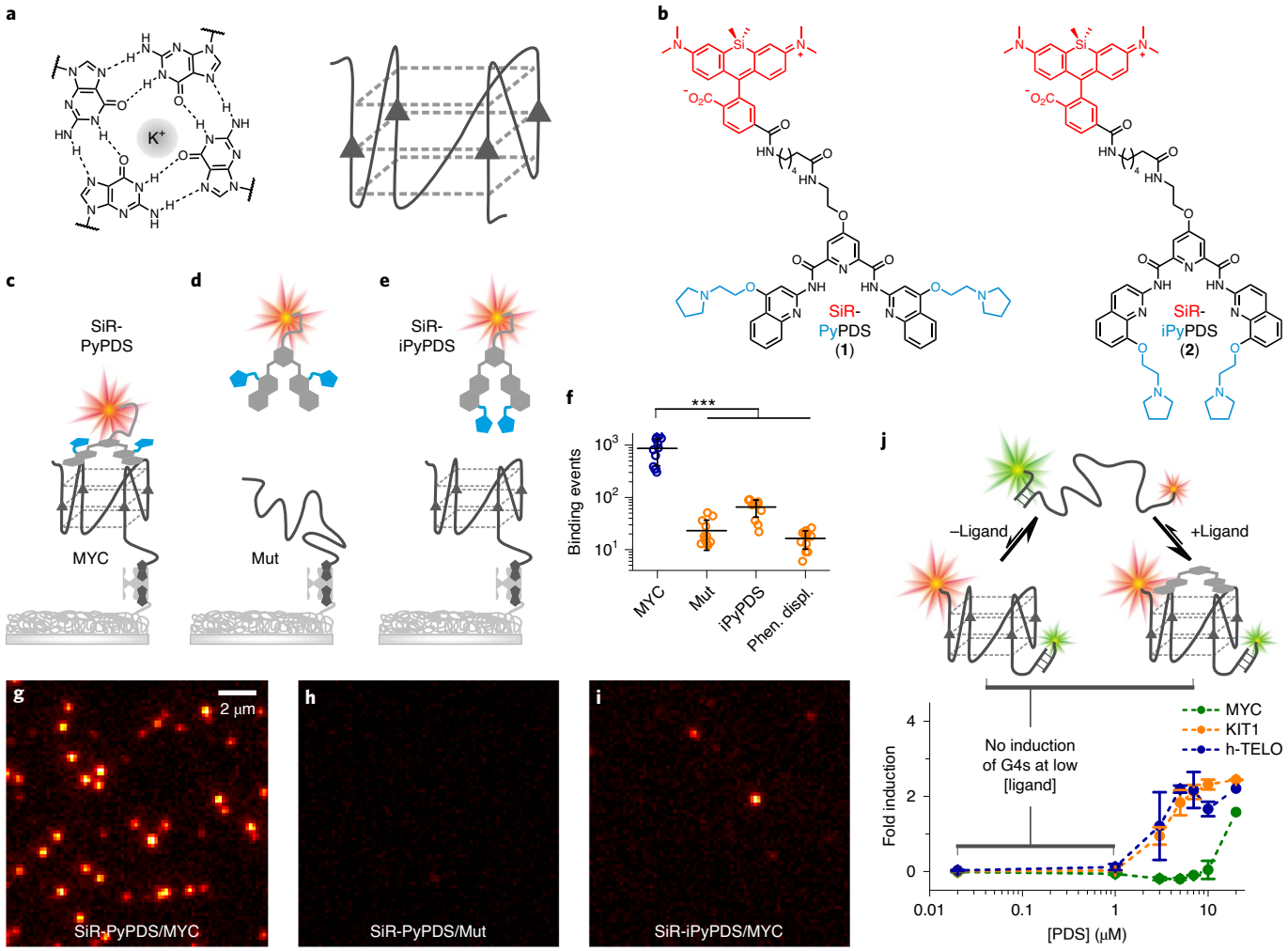

Fig. 1 | In vitro single-molecule fluorescence imaging of G4s. a, Schematic representation of a G-tetrad (left) and a G4 structure (right). **b**, Chemical structures of the selective G4-fluorogenic ligand SiR-PyPDS (**1**) and its inactive isomer, SiR-iPyPDS (**2**). **c**, Schematic of the methodology used for visualizing individual G4s. Pre-folded G4 MYC is attached to a coverslip via a biotin–neutravidin linker. The fluorescent G4 probe SiR-PyPDS (**1**) binds to G4 MYC, which can be visualized using single-molecule fluorescence imaging. **d**, SiR-PyPDS will not bind single-stranded mutated-MYC that cannot form a G4. **e**, The inactive isomer SiR-iPyPDS (**2**), with its 10-fold weaker binding affinity, is less likely to bind G4 MYC. **f**, Quantification of SiR-PyPDS (**1**) binding to the G4 MYC, SiR-PyPDS (**1**) binding to the mutated-MYC (Mut), SiR-iPyPDS (**2**) binding to the G4 MYC and SiR-PyPDS (**1**) binding to the G4 MYC in the presence of 10 µM unlabelled PhenDC3 competitor. Error bars indicate mean ± s.d. $^{***}P < 1 \times 10^{-5}$, unpaired two-sided *t*-test, $n = 12$ measurements from three independent replicates. **g**, Representative images (500-ms exposure) of individual SiR-PyPDS (**1**) molecules (250 pM) binding to a surface coated with pre-folded MYC G4 oligonucleotide. Individual fluorescent puncta indicate binding of single SiR-PyPDS (**1**) molecules. **h**, SiR-PyPDS (**1**) (250 pM) binding to mutated-MYC. **i**, SiR-iPyPDS (**2**) (250 pM) binding to pre-folded MYC. Experiments in **g**–**i** were repeated three times independently with similar results. **j**, Interactions of G4 ligands and G4s can alter the equilibrium between unfolded and folded G4s. Error bars indicate mean ± s.d. $n = 12$ measurements, from three independent replicates. Changes in the Förster Resonance Energy Transfer (FRET) ratio can be observed at micromolar PDS concentrations for c-KIT1 and h-TELO and larger concentrations for MYC, indicative of G4 induction, which does not occur at lower concentrations.

We reasoned that the steric clash of the side chains in SiR-iPyPDS (**2**) could prevent the molecule from adopting the flat conformation required for G-tetrad recognition. Fluorescence titrations confirmed more than a 10-fold lower G4-binding affinity of SiR-iPyPDS (**2**) compared to SiR-PyPDS (**1**) (Supplementary Fig. 3).

Given the promising results from ensemble binding experiments by SiR-PyPDS (**1**) and the negative control analogue SiR-iPyPDS (**2**), we decided to evaluate the suitability of these probes for single-molecule detection of G4s in vitro. To test this, we investigated the binding of SiR-PyPDS (**1**) or SiR-iPyPDS (**2**) to a G4-folded oligonucleotide, MYC, immobilized on a polyethylene glycol (PEG)/biotin-coated surface, by single-molecule imaging (Fig. 1c–e). We acquired images with a long exposure time (500 ms) so as to capture only relatively long-lived interactions. At a much lower ligand concentration than what was used in ensemble experiments (250 pM), we could detect on average of 867 long-lived SiR-PyPDS (**1**) spots (Fig. 1f and Supplementary Video 1) in each field of view (Fig. 1g), but observed a 10-fold reduction in long-lived binding events (66 events, $P = 5 \times 10^{-6}$) for the weaker G4 binder SiR-iPyPDS (**2**) (Fig. 1i and Supplementary Video 1). We confirmed that events represented binding of individual probes to MYC by observing single-step photobleaching (Extended Data Fig. 2). As the MYC sequence was also labelled with Alexa Fluor 488, we could use both Förster Resonance Energy Transer (FRET) and single-molecule FRET (smFRET) (Extended Data Fig. 3) to visualize direct binding of our probe to MYC. Note that, at 250 pM,

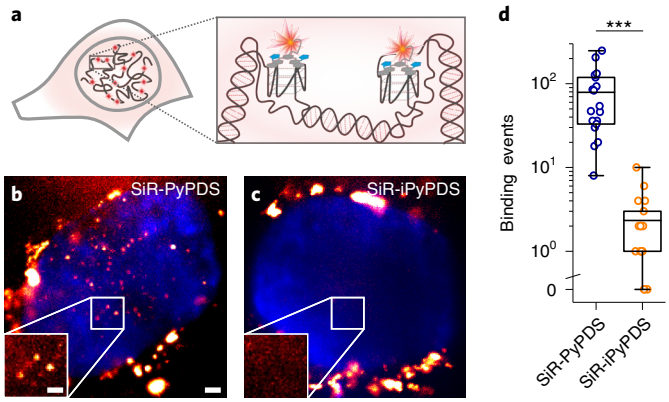

Fig. 2 | Single-molecule fluorescence imaging of G4s in living cells using the fluorescent probe SiR-PyPDS (1). a, Schematic of G4s in the cell nucleus, with a magnified view showing G4s stained by SiR-PyPDS (**1**). **b**, Representative background-subtracted image (max projection of 100 frames with 200-ms exposure) of SiR-PyPDS (**1**) binding events in a living U2OS cell treated with 20 nM SiR-PyPDS (**1**) for 30 min before imaging; fluorescent puncta indicate binding of single SiR-PyPDS (**1**) molecules. Blue colour corresponds to nuclear staining with Hoechst 33342. Scale bars, 2 µm (main image) and 1 µm (inset). **c**, Representative image of SiR-iPyPDS (**2**) staining in a living U2OS cell treated with 20 nM SiR-PyPDS (**1**) for 30 min before imaging. Experiments in **b**,**c** were repeated three times independently, with similar results. **d**, Quantification of the binding events within the nucleus lasting more than two frames (100 ms per frame) per cell for SiR-PyPDS (**1**) and SiR-iPyPDS (**2**). Centre lines indicate the median; boxes show interquartile range; whiskers denote 5th and 95th percentiles. ***$P = 3.5 \times 10^{-7}$, two-sided Mann–Whitney *U*-test, $n = 18$ measurements from six cells each time in three independent replicates.

the labelled fraction, θ, of G4s is ~0.05%, according to the Hill–Langmuir equation $\theta = [L]/(K_d + [L])$, where $[L]$ is the concentration of ligand and K_d is the dissociation constant for ligand binding to G4s. To further investigate whether the number of SiR-PyPDS (**1**) binding events correlates with the density of G4 targets immobilized on the surface, we varied the surface coverage by mixing the biotinylated MYC G4 with a biotinylated ssDNA strand that does not form a G4, at different ratios (see Methods). We observed a linear relationship between the number of SiR-PyPDS (**1**) binding events detected and the concentration of MYC G4 immobilized on the surface, confirming that the number of binding events is proportional to the number of G4s on the surface (Extended Data Fig. 4) and that this number can be used as a proxy for G4 density. We have also confirmed that the MYC sequence used is folded into a G4 structure, as judged by circular dichroism spectroscopy (Supplementary Fig. 4). The observed number of binding events can therefore be used to assess the concentration of folded G4s on the surface. We next compared the binding of SiR-PyPDS (**1**) and SiR-iPyPDS (**2**) to different G4-folding oligonucleotides, including MYC, h-TELO and c-KIT1. Again, we observed a >20-fold increase in the number of binding events for SiR-PyPDS (**1**) when compared to the control probe SiR-iPyPDS (**2**) (Supplementary Fig. 5). These observations confirm that SiR-PyPDS (**1**) can be applied to single-molecule imaging of G4s and that the decreased binding affinity of the control analogue SiR-iPyPDS (**2**) causes the lower number of binding events observed.

To further validate that long-lived binding events observed with SiR-PyPDS (**1**) could be ascribed as G4-specific, we attempted to compete out SiR-PyPDS (**1**) binding to MYC G4 with an excess of the structurally unrelated G4-binding ligand PhenDC3[13]. Gratifyingly, binding of SiR-PyPDS (**1**) to MYC was abrogated when an excess (10 µM) of the potent G4 ligand PhenDC3 was included as a competitor (16 events, $P = 2 \times 10^{-6}$; Fig. 1f and Supplementary Video 2). We also measured the number of binding events displayed by SiR-PyPDS (**1**) when the G4-folding sequence of MYC was mutated to prevent G4 formation. SiR-PyPDS (**1**) binding was negligible (23 events, $P = 2 \times 10^{-6}$) for the immobilized ssDNA control (MYC-mut; Fig. 1f and Supplementary Video 1), which is in agreement with what was observed for SiR-PyPDS (**1**) ensemble fluorescence titrations (Supplementary Fig. 2). Both the biotin-MYC and biotin-MYC-mut used in this experiment were also functionalized with an Alexa-488 fluorophore. We used the 488 emission to measure the total fluorescence on each coverslip functionalized with either MYC or MYC-Mut to ensure comparable densities of oligonucleotides on the surface in the different experiments ($\sigma = 10\%$ variation between coverslips, Extended Data Fig. 4). Therefore, differences observed in binding events were minimally affected by variations in G4 surface coverage, confirming the suitability of the SiR-PyPDS (**1**) and SiR-iPyPDS (**2**) control as probes for the single-molecule detection of G4s.

We next sought to determine whether the conditions of relatively low probe concentrations used for single-molecule imaging caused global induction of G4 folding or perturbation of G4-folding dynamics. To investigate this, we used G4-folding oligonucleotides (MYC, h-TELO and c-KIT1) labelled with a Cy5 fluorophore at their 5′ end and having an overhang hybridized with a complementary oligonucleotide sequence containing a Cy3 fluorophore at their 3′ end. The oligonucleotides form a Cy3–Cy5 FRET system capable of assessing the fraction of folded G4s by measuring the FRET efficiency between the two fluorophores[14]. When titrated with increasing concentrations of PyPDS, no significant FRET perturbation was observed for PyPDS concentrations below 3 µM (Extended Data Fig. 5). Therefore, there is no detectable global induction of G4s when imaging under low nanomolar concentrations (Fig. 1j), as opposed to the induction caused by exposure to micromolar concentrations of the ligand. We studied G4-unfolding dynamics using a FRET system with a 5′ carboxyfluorescein (FAM) and a 3′ carboxytetramethyl-rhodamine (TAMRA) labelled oligonucleotides that were annealed in 150 mM K^+ to form a stable G4 structure (see Methods). We next added a 10-fold molar excess of DNA sequence complementary to the G4-folding sequence to irreversibly trap the unfolded G4 sequence as dsDNA. This allowed us to measure the unfolding kinetics by monitoring a concomitant decrease in the FRET fluorescence signal, as previously described[14]. We found that micromolar concentrations of SiR-PyPDS (**1**) are required to slow down the unfolding rate for the tested G4 structures and that low nanomolar concentrations used for single-molecule experiments do not globally affect the unfolding rate of the tested G4 structures (Extended Data Fig. 6). Our data demonstrate that single-molecule imaging can be used to address the pervasive problem of current G4-detection strategies that use relatively high concentrations of affinity probes that might globally perturb G4 folding and dynamics.

We next applied the fluorescent G4 ligands to single-molecule imaging of G4s in live cells (Fig. 2a). First, we investigated the toxicity of SiR-PyPDS (**1**) and SiR-iPyPDS (**2**) in U2OS cells over a 24-h treatment at different probe concentrations. Neither SiR-PyPDS (**1**) nor SiR-iPyPDS (**2**) elicited any cell death response at nanomolar concentrations, as toxicity could only be observed at concentrations higher than 10 µM (Supplementary Fig. 6). Based on this, U2OS cells were treated for 30 min with 20 nM SiR-PyPDS (**1**), which resulted in under-labelling of G4s at a density where individual fluorophores were spatially well separated (Fig. 2b). This allowed us to visualize individual probes (SiR-PyPDS (**1**) or SiR-iPyPDS (**2**)) binding to targets in the nucleus (Fig. 2b,c and Supplementary Video 3) using single-molecule imaging (400 frames taken with 100-ms exposure using highly inclined laminated optical sheet (HILO) microscopy)[15]. Single-step photobleaching provided evidence of binding events by

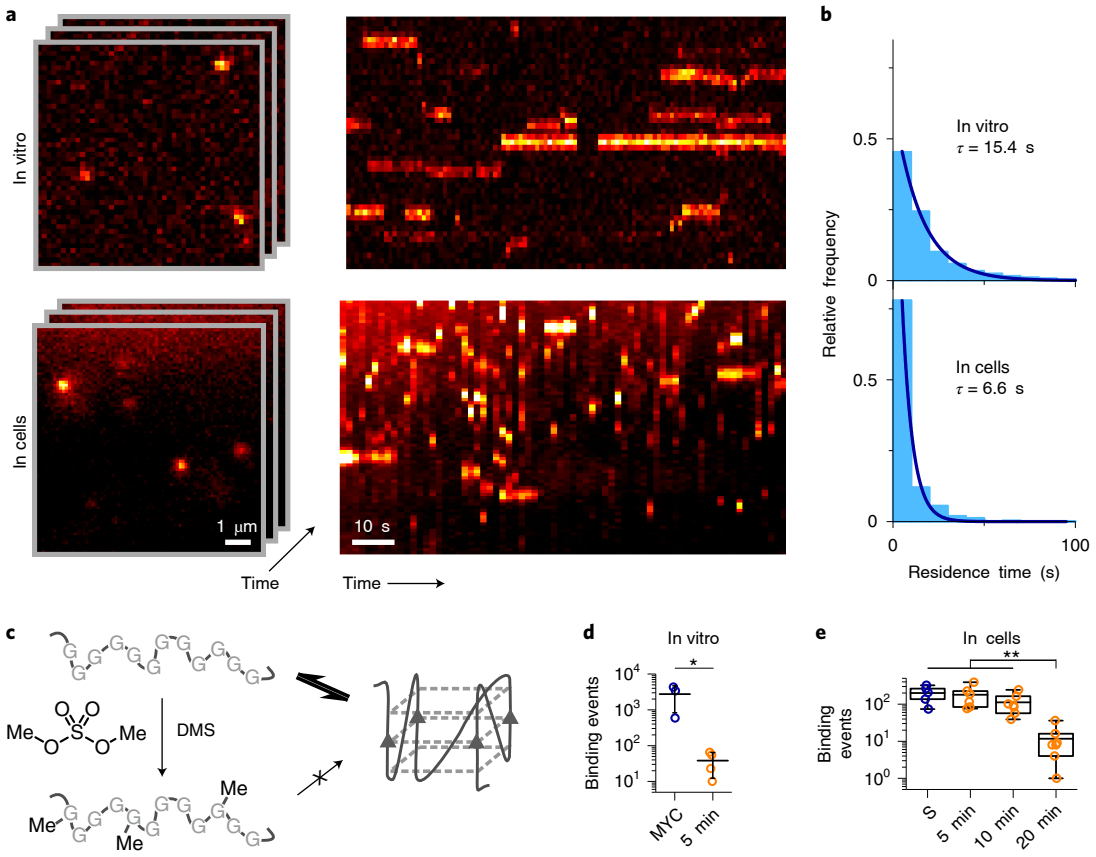

Fig. 3 | G4s in living cells undergo dynamic folding and unfolding. a, Single-molecule time-lapse imaging of SiR-PyPDS (**1**) in vitro (top) and in cells (bottom). Individual images from the time-lapse stack are shown on the left, while kymographs on the right show the dynamic binding kinetics of SiR-PyPDS (**1**) to G4s. The experiments were repeated three times independently, with similar results. **b**, The histograms of dwell times for each experiment (three positions on a coverslip for in vitro experiments and six cells for the cell experiment) were fitted with a single exponential fit to determine the binding lifetime in each condition. **c**, Schematic of DMS-meditated chemical trapping of unfolded G4s. **d**, Quantification of G4-binding events for untreated and 600 mM DMS-treated G4 MYC for 20 min. Error bars indicate mean ± s.d. $^{*}P = 0.05$, two-sided Mann–Whitney *U*-test. $n = 3$ (MYC) and $n = 4$ (DMS) measurements taken from three independent replicates. **e**, Quantification of G4-binding events detected in living cells upon increased exposure to DMS (20 mM), showing a clear time-dependent depletion of G4s. Centre lines indicate the median; boxes show interquartile range; whiskers denote 5th and 95th percentiles. $^{**}P < 0.01$, two-sided Mann–Whitney *U*-test. $n = 5$, 6, 7 and 8 cells for untreated, 5 min, 10 min and 20 min, respectively, taken from three independent replicates.

individual probe molecules in the nucleus (Extended Data Fig. 7), in spite of the extra-nuclear lysosomal accumulation of SiR-PyPDS (**1**) (Extended Data Fig. 8). We first measured the number of binding events where a SiR-PyPDS (**1**) molecule remained stationary within a 300-nm radius for three or more consecutive frames (that is, 300 ms), detecting an average of 79 binding events per nuclei over 40 s of imaging (Fig. 2d). Similar to observations in vitro, treatment of U2OS cells with SiR-iPyPDS (**2**) (20 nM) revealed an average of only two long-lived binding events in the nucleus (Fig. 2d). To confirm that differences in the number of nuclear binding events between SiR-PyPDS (**1**) and SiR-iPyPDS (**2**) were not due to different cellular uptake of the two ligands, we used confocal microscopy and demonstrated that, with 10 μM ligand treatment, the total nuclear fluorescence intensity measured was comparable for the SiR-PyPDS (**1**) and SiR-iPyPDS (**2**) treatments (Extended Data Fig. 9). These results are consistent with the in vitro observations (Fig. 1f) and corroborate the hypothesis that long-lived SiR-PyPDS (**1**) binding events could be ascribed to specific G4 binding in cells. To further support this hypothesis, we demonstrated that SiR-PyPDS (**1**) binding could be abrogated in the presence of 10 μM of the unlabelled competitor G4 ligands PDS[12] or PhenDC3[13] (Extended Data Fig. 10 and Supplementary Video 4), which is also consistent with observations in vitro.

We next sought to estimate the fraction of G4 labelled by SiR-PyPDS (**1**) in living cells, as done for the in vitro studies. To do so, we assumed that the K_d of SiR-PyPDS (**1**) remains unchanged in the cellular environment and that the nuclear concentration of the probe is 20 nM. Based on these assumptions and using the relationship $[L]/(K_d + [L])$, the fraction of labelled G4s on a single U2OS cell is ~4%. Using this value for the labelled G4 fraction, we roughly estimated the total number of G4s present in a single cell. As we detect ~10 binding events on average in an image frame within a single focal plane (~1 μm), there would be ~100 binding events in an entire U2OS nucleus with diameter of ~10 μm. Therefore, considering we are labelling ~4% of the total number of targets, we can estimate a total number of G4s in a single cell of ~3,000, which is in line with what has been detected in human chromatin (between 1,000 and 10,000 G4s) in G4 ChIP-Seq experiments[6].

We then compared the temporal dynamics of the interaction between SiR-PyPDS (**1**) and G4s in vitro and in cells, to investigate if the characteristic dwell times of SiR-PyPDS (**1**) binding to G4s in vitro could also be detected in cells. Time-lapse imaging was used

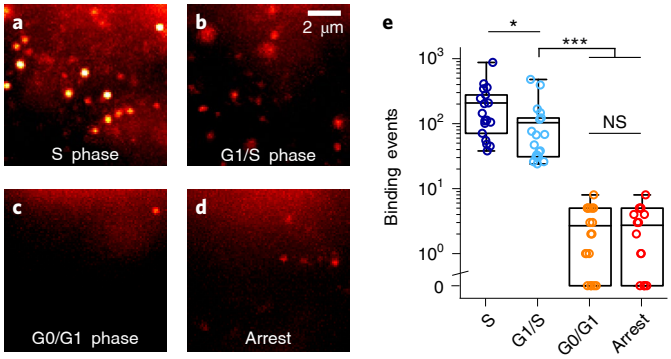

Fig. 4 | The observation of G4s in live cells is altered by cell-cycle phase and transcription. a–d, Representative single-molecule images of G4-binding events are shown for synchronized U2OS cells in the S phase (**a**), G1/S phase (**b**) and G0/G1 phase (**c**) and for unsynchronized cells treated with both the transcriptional inhibitor DRB and the replication inhibitor aphidicolin (**d**). Experiments **a–d** were repeated three times independently, with similar results. **e**, Quantification of binding events lasting more than two frames (100 ms per frame) per cell in living U2OS cells at different cell-cycle phases and after transcription/replication arrest. Centre lines indicate the median; boxes show interquartile range; whiskers denote 5th and 95th percentiles. $^{***}P<1\times10^{-6}$; $^{*}P=0.01$; NS, $P=0.99$; two-sided Mann–Whitney U test. $n=18$, 19, 19 and 15 cells for S, G0, G1 and arrest, respectively, taken from three independent replicates.

to observe long-lived events (Fig. 3a and Supplementary Video 5). In vitro, an exposure time of 100 ms and interval of 2 s were used to avoid photobleaching effects (time constant $\tau_b=923$ s), whereas for cellular experiments a slightly longer interval (3 s, $\tau_b=104$ s) and a longer exposure time (500 ms) were needed to limit contributions from unbound ligands[16]. The histogram of SiR-PyPDS (**1**) dwell times could be fitted well ($R^2>0.99$) to a single exponential distribution, yielding a photobleaching-corrected binding lifetime of 6.6 ± 0.5 s in cells (Fig. 3b), which is significantly shorter (~2.5 fold, $P=4\times10^{-7}$, unpaired *t*-test) than that observed in vitro for binding (15.4 ± 0.6 s) to MYC G4. To investigate further this apparent discrepancy, we carried out in vitro binding experiments with other G4-forming sequences. These experiments indicated that the dwell times for SiR-PyPDS (**1**) binding to h-TELO and c-KIT1 were respectively 2.5 and 2 times shorter than MYC and were comparable to the dwell times observed in living cells. These experiments suggested that the binding dynamics of SiR-PyPDS (**1**) to synthetic G4-forming oligonucleotides observed in vitro can be recapitulated in cells, further supporting that our assay can detect endogenous G4s.

To gain insight into the G4-folding dynamics in living cells, we employed the DNA-methylating agent dimethyl sulfate (DMS) to irreversibly trap the unfolded G4 state (Fig. 3c). The nucleophilic N7 atoms of guanines are exposed and can be methylated by DMS in ssDNA and dsDNA, but are protected in folded G4s by their participation in Hoogsteen hydrogen bonding (Fig. 1a). Thus, transiently unfolded G4s can be methylated and irreversibly prevent further G4 refolding by blocking Hoogsteen hydrogen bonding at N7s (Fig. 3c). First, we demonstrated that DMS could trap the unfolded G4 state in vitro by quantifying binding events of SiR-PyPDS (**1**) with MYC before (300 events) and after (40 events, $P=0.03$) 20 min treatment with 640 mM (8%) DMS over 30 s of imaging (Fig. 3d). We then examined if a similar DMS-dependent G4 depletion could be recapitulated in living cells, while keeping the DMS concentration lower (20 mM, 0.25%) to prevent cell death. We observed a time-dependent decrease of SiR-PyPDS (**1**) binding events in U2OS cells within minutes after DMS treatment (Fig. 3e and Supplementary Video 6), with an ~20-fold reduction ($P=0.006$) in binding events after 20 min exposure. These results suggest that G4s naturally undergo structural fluctuations in cells. This, in turn, makes their specific detection by chemical methods, such as DMS-Seq[17], ineffective, as they will inevitably trap the unfolded state (Fig. 3c).

We also probed the dynamic formation of G4s in live U2OS cells through different phases of the cell cycle to gain insights into changes in G4 prevalence during active DNA processing states, such as replication (S phase) and transcription (G1 phase). We first confirmed, using confocal microscopy, that under different tested conditions there were negligible differences in uptake of the fluorescent G4 ligand (Extended Data Fig. 9). This ensured that the lack of binding events observed under certain cycle phases or after DMS treatment could be confidently ascribed to a change in G4 prevalence. U2OS cells treated with SiR-PyPDS (**1**) were synchronized to S, G1/S and G0/G1 phases using previously reported procedures[4] and imaged using single-molecule fluorescence microscopy. During S phase, where the cell is undergoing active replication, significant ($P<1\times10^{-6}$) binding events could be detected over 40 s of imaging (208 events; Fig. 4a and Supplementary Video 7). The number of binding events was slightly reduced (103 events, $P=0.01$) when cells were preparing to initiate replication (G1/S phase) and transcription was active (Fig. 4b and Supplementary Video 7). There were negligible ($P<1\times10^{-6}$) binding events during G0/G1 phase over 40 s of imaging (three events; Fig. 4c and Supplementary Video 7), where cellular processes are quiescent. These results show that G4 formation is associated with both transcription and replication and are in agreement with previous observations reported in fixed cells[4,18]. To further confirm the suppression of G4s in the absence of actively processed DNA, we treated unsynchronized U2OS cells with a global replication inhibitor (aphidicolin) and also the global transcription inhibitor 5,6-dichloro-1-β-D-ribofuranosylbenzimidazole (DRB), as previously described[18], to mimic the quiescent state that characterizes cells undergoing G0 phase. Upon transcription and replication arrest, few binding events were detected over 40 s of imaging (three events, $P<1\times10^{-6}$), further demonstrating that actively processed DNA is pivotal for G4 formation in living cells (Fig. 4c,d and Supplementary Video 7).

We have used fluorescent probe molecules to visualize individual G4 structures in living cells using single-molecule fluorescence imaging. The sensitivity of single-molecule methods enabled us to image individual binding events to G4 structures at probe concentrations orders of magnitude lower than normally used in biophysical and cellular experiments, thereby minimizing global perturbation of G4s. We applied our new imaging platform to demonstrate that G4 formation is cell-cycle-dependent and that the presence of G4s is directly related to fundamental biological processes such as active transcription and replication, as chemical inhibition of these processes led to abrogation of detectable G4s in living cells. Trapping of unfolded G4s by means of DMS methylation revealed that G4s undergo dynamic fluctuations in live cells and that essentially all G4s are trapped in the unfolded state during the course of 20 min of DMS treatment (0.25%, 20 mM). We anticipate that further application of this imaging platform will help unravel specific biological functions regulated by individual G4s within the human genome, in real time.

Online content

Any methods, additional references, Nature Research reporting summaries, source data, extended data, supplementary information, acknowledgements, peer review information; details of author contributions and competing interests; and statements of data and code availability are available at https://doi.org/10.1038/s41557-020-0506-4.

Received: 15 February 2019; Accepted: 9 June 2020;
Published online: 20 July 2020

References

1. Sen, D. & Gilbert, W. Formation of parallel four-stranded complexes by guanine-rich motifs in DNA and its implications for meiosis. *Nature* **334**, 364–366 (1988).
2. Hänsel-Hertsch, R., Di Antonio, M. & Balasubramanian, S. DNA G-quadruplexes in the human genome: detection, functions and therapeutic potential. *Nat. Rev. Mol. Cell Biol.* **18**, 279–284 (2017).
3. Chambers et al. High-throughput sequencing of DNA G-quadruplex structures in the human genome. *Nat. Biotechnol.* **33**, 877–881 (2015).
4. Schaffitzel, C. et al. In vitro generated antibodies specific for telomeric guanine-quadruplex DNA react with Stylonychia lemnae macronuclei. *Proc. Natl Acad. Sci. USA* **98**, 8572–8577 (2001).
5. Biffi, G., Tannahill, D., McCafferty, J. & Balasubramanian, S. Quantitative visualization of DNA G-quadruplex structures in human cells. *Nat. Chem.* **3**, 182–186 (2013).
6. Hänsel-Hertsch, R. et al. G-quadruplex structures mark human regulatory chromatin. *Nat. Genet.* **48**, 1267–1272 (2016).
7. Chen, X. C. et al. Tracking the dynamic folding and unfolding of RNA G-quadruplexes in live cells. *Angew. Chem. Int. Ed.* **57**, 4702–4706 (2018).
8. Laguerre, A. et al. Visualization of RNA G-quadruplexes in live cells. *J. Am. Chem. Soc.* **137**, 8521–8525 (2015).
9. Zhang, S. et al. Real-time monitoring of DNA G-quadruplexes in living cells with a small-molecule fluorescent probe. *Nucleic Acids Res.* **46**, 7522–7532 (2018).
10. Shivalingam, A. et al. The interactions between a small-molecule and G-quadruplexes are visualized by fluorescence lifetime imaging microscopy. *Nat. Commun.* **6**, 8178 (2015).
11. Lukinavičius, G. et al. A near-infrared fluorophore for live-cell super-resolution microscopy of cellular proteins. *Nat. Chem.* **5**, 132–139 (2013).
12. Rodriguez, R. et al. A novel small molecule that alters shelterin integrity and triggers a DNA-damage response at telomeres. *J. Am. Chem. Soc.* **130**, 15758–15759 (2008).
13. De Cian, A., Delemos, E., Mergny, J. L., Teulade-Fichou, M. P. & Monchaud, D. Highly efficient G-quadruplex recognition by bisquinolinium compounds. *J. Am. Chem. Soc.* **129**, 1856–1857 (2007).
14. Ying, L., Green, J. J., Li, H., Klenerman, D. & Balasubramanian, S. Studies on the structure and dynamics of the human telomeric G-quadruplex by single-molecule fluorescence resonance energy transfer. *Proc. Natl Acad. Sci. USA* **100**, 14629–14634 (2003).
15. Tokunaga, M., Imamoto, N. & Sakata-Sogawa, K. Highly inclined thin illumination enables clear single-molecule imaging in cells. *Nat. Methods* **5**, 159–161 (2008).
16. Etheridge, T. J. et al. Quantification of DNA-associated proteins inside eukaryotic cells using single-molecule localization microscopy. *Nucleic Acids Res.* **42**, e146 (2014).
17. Guo, J. U. & Bartel, D. P. RNA G-quadruplexes are globally unfolded in eukaryotic cells and depleted in bacteria. *Science* **353**, aaf537 (2016).
18. Rodriguez, R. et al. Small-molecule-induced DNA damage identifies alternative DNA structures in human genes. *Nat. Chem. Biol.* **8**, 301–310 (2012).

Methods

Detailed synthetic protocols and purification methodologies for the preparation of SiR-PyPDS (**1**), SiR-iPyPDS (**2**), SiR-C4-PyPDS (**3**) and SiR-C8-PyPDS (**4**), biophysical methods and more detailed protocols are described in the Supplementary Information.

Fluorescence titrations. Before every experiment, individual fresh 25 µM solutions of oligo (MYC, h-TELO, c-KIT1, MYC-mutant and dsDNA) and a 200 nM solution of SiR-PyPDS (**1**) or SiR-iPyPDS (**2**) were prepared in assay buffer (100 mM KCl and 50 mM KH_2PO_4, pH 7.4). Oligonucleotides were annealed by heating the solution in buffer at 95 °C for 10 min followed by a slow cool down at room temperature. Annealed oligos were then preserved at 4 °C overnight before being used for fluorescence titrations.

In a typical experiment, 50 µl of a 25 µM oligo solution was placed in a 96-well black plate and diluted (1:1) through 11 of the 12 wells of the plate row. No oligo was added in the last well to act as negative control. Successively, 50 µl of the 200 nM SiR-PyPDS (**1**) analogue solution was added to every well. The wells were sealed with adhesive foil, covered with aluminium foil and placed on an orbital plate shaker for gentle agitation at room temperature for 2 h. End-point fluorescence (at 633 nm) of each well was measured on a fluorescence plate reader (BMG PHERAstar Plus). The data are plotted as the ratio of the fluorescence intensity emission of each SiR compound (100 nM) measured at 633 nm at every titration point over the fluorescent emission measured at 633 nm for the same SiR analogue (100 nM) in buffer only and normalized to the highest fluorescence emission value measured per oligonucleotide studied, which defines 100% molecule bound. Measurements were performed in triplicate.

Spectroscopic characterization of SiR-PyPDS. A 20 µM SiR-PyPDS (**1**) solution was prepared in K^+ buffer (50 mM KH_2PO_4, 100 mM KCl, 58 mM LiOH, pH 7.4) and its absorbance and fluorescence spectra were measured. Serial dilution and measurement cycles were repeated down to a 0.63 µM concentration of SiR-PyPDS (**1**). Myc oligo was diluted to 10 µM solutions in K^+ buffer and annealed at 95 °C for 10 min, then slowly cooled to room temperature and stored at 4 °C. SiR-PyPDS (**1**) (10 µM) was prepared in K^+ buffer with 10 µM Myc oligo and absorbance and fluorescence of the solution were measured. Serial dilution of SiR-PyPDS (**1**) and measurement cycles were repeated down to a concentration of 1.3 µM of SiR-PyPDS (**1**), keeping the Myc oligo concentration constant at 10 µM.

Fluorescence excitation and emission spectra were recorded on Duetta fluorescence and absorbance spectrometer (Horiba Scientific) at room temperature. Absorption was measured in 300–800-nm intervals with 1-nm step size and 1-nm bandwidth. Fluorescence spectra were recorded by exciting at 625 nm and measuring the 630–800-nm range with a 5-nm excitation slit and 5-nm emission slit.

The fluorescence quantum yield (Φ) of SiR-PyPDS (**1**) and SiR-PyPDS (**1**) bound to Myc G4 was determined via the following model:

$$\Phi = \Phi_R \left(\frac{\int I1 - 10^{-A_R} n^2}{\int I_R 1 - 10^{-A} n_R^2} \right)$$

where Φ_R is the fluorescence quantum yield of Cresyl Violet, which was used as a standard. I and I_R are the fluorescence intensities of SiR and Cresyl Violet, respectively. A and A_R are the absorbances of SiR and Cresyl Violet, respectively. n is the refractive index of the K^+ buffer used for SiR (1.33) and n_R is the refractive index of ethanol (1.36).

SiR-PyPDS analogue G4-binding comparison. To compare the fluorescence 'light-up' of the different SiR-PyPDS analogues (**1**, **3** and **4**), we measured the fluorescence emission of SiR in the presence of different G4 folded oligonucleotides. In a typical experiment, the fluorescence intensity at 633 nm was measured in the presence of SiR compounds and G4 oligo at final concentrations of 100 nM and 10 µM, respectively. The experiments were performed in 96-well black plates with a total volume of 100 µl and conducted in triplicate. The wells were sealed with an adhesive foil cover, covered with aluminium foil and placed on an orbital plate shaker for gentle agitation at room temperature for 2 h. End-point fluorescence at 633 nm of each well was measured on a fluorescence plate reader (BMG PHERAstar Plus). The data are plotted as the ratio of the fluorescence intensity emission of each SiR compound (100 nM) measured by exciting the probe at 633 nm in the presence of 10 µM G4 oligos (c-Myc, h-TELO and c-KIT1),over the fluorescent emission measured at 633 nm for the same SiR analogue (100 nM) in buffer only. Experiments were performed in triplicate.

G4 unfolding kinetics. Stock solutions of 2 µM FRET h-TELO and c-KIT1 oligonucleotides and 20 µM h-TELO and c-KIT1 complementary oligonucleotides were prepared separately in K^+ buffer (50 mM KH_2PO_4, 100 mM KCl, 58 mM LiOH, pH 7.4) and annealed at 95 °C for 10 min, then slowly cooled to room temperature and stored in the dark at 4 °C. The samples were then mixed and excited at a wavelength of 493 nm via a 5-nm excitation slit and emission was measured at 518 nm via a 5-nm emission slit. The detector voltage was 570 V for the h-TELO FRET oligo and 650 V for the c-KIT1 oligo. Data points were taken every 2 min for 20 h with 5 s of read averaging. Kinetic runs were initiated by mixing 50 µl of 2 µM FRET oligo with 50 µl of 20 µM complementary trap oligo at $t = 0$ min and oligo unfolding progression was followed by the increase of FAM fluorescence signal at 518 nm. Kinetics data were recorded using Cary Kinetics software and analysed using Prism. Kinetics curves were fitted with a two-phase association model.

G4 induction measurements. Stock solutions of FRET2 h-TELO, FRET2 Myc and FRET2 c-KIT1 at 1 µM were mixed with FRET2 comp overhang Cy3 oligo (Supplementary Table 1) in 10 mM Tris buffer and annealed at 95 °C for 10 min, then allowed to cool to room temperature and stored at 4 °C overnight. The samples were excited at a wavelength of 540 nm via a 5-nm excitation slit and emission was measured at 550–750 nm via a 5-nm emission slit. The detector voltage was set to 600 V. h-TELO, Myc and c-KIT1 FRET systems at 1 µM concentration were studied by titrating in PyPDS from a concentrated stock solution in water followed by fluorescence measurements. Data were analysed using Prism software. Fold induction was calculated according to

$$\text{Fold induction}_i = \frac{\frac{F(Cy5)_i}{F(Cy3)_i} - \frac{F(Cy5)_0}{F(Cy3)_0}}{\frac{F(Cy5)_0}{F(Cy3)_0}}$$

where $F(Cy5)_i$ and $F(Cy3)_i$ denote the respective dye fluorescence intensity peak maxima at a particular PDS concentration and $F(Cy5)_0$ and $F(Cy3)_0$ denote the respective dye fluorescence intensity in the absence of PDS.

Bulk SiR-PyPDS (1) and MYC-488 FRET titration. A fresh 1 µM solution of MYC-488 (same sequence as used for the in vitro surface experiments) was prepared by annealing in assay buffer (100 mM KCl and 50 mM KH_2PO_4, pH 7.4). MYC-488 was annealed by heating the solution at 95 °C for 10 min followed by slow cool down at room temperature and left at 4 °C overnight before being used for FRET titrations.

In a typical experiment, 500 µl of a 1 µM MYC-488 solution was placed in a quartz cuvette and the emission spectra were recorded while exciting the sample at 488 nm and recording the emission between 500 and 700 nm with a 5-nm emission slit. Successively, SiR-PyPDS (**1**) was added (0.5 to 5 µl) from a 1 mM stock solution in the assay buffer (10% DMSO). Spectra were recorded under the same conditions after each SiR-PyPDS (**1**) addition and FRET between the MYC-488 and SiR was detected by assessing the intensity reduction of the emission of the 488 fluorophore (peak ~515 nm) followed by the increased emission of SiR (peak ~625 nM).

smFRET imaging. Biotinylated oligonucleotides (MYC) were added to PEG-coated surfaces as described in the main text. To directly visualize smFRET between the Alexa Fluor 488 tag on c-MYC and SiR-PyPDS (**1**) upon binding to c-MYC, we captured two images of SiR-PyPDS (**1**) emission: (1) under donor (488 nm) excitation (200 W cm^{-2}) to observe FRET and (2) under acceptor (647 nm) excitation (150 W cm^{-2}) to observe all PyPDS molecules bound to the surface. A separate set of smFRET experiments were also carried out at a 1,000-fold lower concentration of c-MYC (0.001% surface coverage) and higher concentrations of SiR-PyPDS (**1**) (10 nM) to monitor anti-correlated donor and acceptor emission.

PEG coating method 1. Coverslips (22 × 22 mm, thickness 0.13–0.17 mm, Menzel Gläser) were first cleaned with argon plasma for at least 1 h (Femto Plasma Cleaner; Diener Electronic) and then attached to a 9-well PDMS chamber (cut from a CultureWell chambered coverglass; Sigma, cat. no. GBL103350-20EA). Each well was passivated with 10 µl of a 4:1 mixture of methoxy- (0.8 mg ml^{-1}; SuSoS, cat. no. PLL(20)-g[3.5]-PEG(2)) and biotin-terminated (0.2 mg ml^{-1}; SuSoS, cat. no. PLL(20)-g[3.5]-PEG(2)/PEG(3.4)-biotin(50%)) PLL/PEG grafted co-polymers in 1× phosphate buffered saline (PBS) for 30 min. The wells were then washed twice with 10 µl of 1× PBS containing 0.05% Tween-20 (Fisher BioReagents, cat. no. 10113103), then treated with 10 µl of 1× PBS containing 1% Tween-20 for 10 min.

PEG coating method 2. Glass coverslips (22 × 22 mm, thickness 0.13–0.17 mm, VWR) were covalently PEGylated, largely according to an existing protocol[19], with minor modifications. Briefly, coverslips were washed, then etched by sonication (Ultrasonic cleaner USC100T, VWR), in a series of solvents (10 min in each of 18.2-MΩ cm^{-1} water, acetone, then MeOH, followed by 20 min in 1 M KOH), rinsed with MeOH, 18.2-MΩ cm^{-1} water, then MeOH, dried in a stream of nitrogen, then cleaned with argon plasma for 15 min (Femto Plasma Cleaner; Diener Electronic). The surfaces were then silanized with 1.5 ml of 3-aminopropyl triethoxysilane (Fisher Scientific UK, cat. no. 10677502), 2.5 ml of AcOH in ~60 ml of MeOH for 20 min, with 30 s of sonication after 10 min. The coverslips were then rinsed with MeOH, 18.2-MΩ cm^{-1} water, then MeOH, dried in a stream of nitrogen and then attached to a 9-well PDMS chamber (cut from a CultureWell chambered coverglass, Sigma, cat. no. GBL103350-20EA). Each well was passivated by adding 9 µl of a 100:1 aqueous mixture of methoxy- (110 mg ml^{-1}, ~22 mM, M_w ~5,000; Laysan Bio Inc., cat. no. MPEG-SVA-5000) and biotin-terminated (1.1 mg ml^{-1}, ~220 µM, M_w ~5,000, Laysan Bio Inc., cat. no. Biotin-PEG-SVA-5000) PEGs, each activated at the other terminus as the *N*-hydroxysuccinimidyl ester, before adding 1 µl of 1 M $NaHCO_3$ (pH 8.5). After overnight incubation in a humid chamber, the coverslips were rinsed well with 18.2-MΩ cm^{-1} water and dried with a stream of nitrogen. Each well was then further passivated by adding 9 µl of an aqueous solution of a shorter, methoxy-terminated PEG, activated at the other

terminus as the *N*-hydroxysuccinimidyl ester (10 mg ml^{-1}, 30 mM, MS(PEG)4 methyl-PEG-NHS-Ester; ThermoFisher, cat. no. 22341), before adding 1 µl of 1 M $NaHCO_3$ (pH 8.5). The coverslips were again incubated overnight in a humid chamber, rinsed well with 18.2-MΩ cm^{-1} water, dried with a stream of nitrogen, then stored in a desiccator at −20 °C until needed.

Quantification of binding events. For in vitro binding event measurements, the number of events was determined by counting the number of peaks in an image using the 'Find Maxima' function in ImageJ with a noise threshold of 5,500. For binding event measurements in cells, a single image typically only yielded a few points, so it was necessary to acquire a video to obtain a suitable number of binding events. Before analysis, a rolling ball background subtraction of 5 px and a 1-px Gaussian blur were applied to all images. Single-molecule tracking was then performed using TrackMate[20], with the particle diameter set to 5 px, threshold set to 200, linking distance set to 3 px, gap closing distance set to 3 px and gap frames set to 3. The number of binding events was then quantified as the number of tracks with a track length of three or longer.

In vitro single-molecule fluorescence imaging. Binding of G4 ligands to synthetic biotinylated oligonucleotides was imaged at single-molecule resolution by total internal reflection fluorescence microscopy (TIRFM) on glass coverslips coated with PEG and NeutrAvidin. In this study, we used two different PEG coating procedures described above: one based on passive adsorption (coating method 1, used for data in Figs. 1 and 3 and Extended Data Fig. 2) and the other on covalent coupling (coating method 2, used for data in Extended Data Figs. 3 and 4 and Supplementary Fig 5). We found similar surface densities of immobilized biotinylated oligonucleotides and degrees of non-specific binding on each surface. Buffers for surface treatment and imaging were freshly filtered each day (0.02-µm syringe filter; Whatman, cat. no. 6809–2101). Each biotinylated surface was then treated in the same way before single-molecule imaging. Wells were first coated with 10 µl of 0.2 mg ml^{-1} NeutrAvidin (ThermoFisher, cat. no. 31000) in 1× PBS containing 0.05% Tween-20 for 5 min, washed twice with 10 µl of 1× PBS containing 0.05% Tween-20, then treated with 10 µl of 1× PBS containing 1% Tween-20 for 10 min. Biotinylated oligonucleotides (c-MYC or c-MYC-mutant, annealed overnight at 100 nM concentration in 100 mM KCl and 50 mM KH_2PO_4, pH 7.4) were then diluted to 10 nM in 1× PBS containing 0.05% Tween-20 and 10 µl was added to each well for 5 min. The wells were then washed twice with 10 µl of 1× PBS containing 0.05% Tween-20, then treated with 10 µl of 1× PBS containing 1% Tween-20 for 10 min. The wells were then washed once with 250 pM of G4 ligand solutions (SiR-PyPDS (**1**) or SiR-iPyPDS (**2**)) in PBS and the solution was finally replaced with 9 µl of G4 ligand at 250 pM in PBS. For in vitro ligand displacement experiments, 1 µl of 1 mM PhenDC3 was added to the well. For DMS trapping, the pre-annealed MYC oligonucleotide (100 nM) was treated with DMS 8% for 20 min, quenched by adding 10% β-mercapto-ethanol and used for surface coating.

The general set-up used for TIRFM has been described previously[21]. For the in vitro experiments, TIRFM was implemented on a Nikon Eclipse Ti2 inverted microscope with a Perfect Focus System for maintaining focus during acquisition. We used 488-nm (MLD 488-200, Cobolt) and 640-nm (LBX-638-180-CSB-PP, Oxxius) lasers for excitation with clean-up filters. The emission collected by the 1.49-NA oil immersion ×60 (×90 with internal magnification) objective lens (Nikon) was filtered with long-pass and band-pass filters (520/36 – 67030 and 692/40 – 67038, Edmund Optics) and imaged on an Evolve 512 Delta electron-magnifying charge-coupled device (Photometrics) with a pixel size of 178 nm, confirmed using a Ronchi ruling. The excitation power density was measured by determining the excitation power after the objective and the beam size in the imaging plane, taking approximately fourfold near-field enhancement into account. For binding event measurements, a field of view was acquired for each condition with 500-ms exposure time at a power density of 1.4 kW cm^{-2}. For longer residency time measurements, time lapses of 300 frames were acquired every 2 s with an exposure time of 100 ms and a power density of 0.4 kW cm^{-2}. For shorter residency time measurements, time lapses of 300 frames were acquired every 100 ms with an exposure time of 100 ms and a power density of 0.4 kW cm^{-2}.

Live-cell imaging. In a typical experiment ~200,000 U2OS cells diluted in 2 ml of Dulbecco's modified Eagle medium (DMEM) were plated in a 35-mm dish with a 14-mm glass coverslip at the bottom (MatTek), then allowed to adhere overnight. After ~18 h, the medium was replaced with 2 ml of fresh DMEM medium containing SiR-PyPDS (**1**) or SiR-iPyPDS (**2**) at a final concentration of 20 nM, then cells where further incubated for 30 min. The DMEM medium containing SiR molecules was then discarded and cells were washed twice with PBS pre-warmed at 37 °C. Finally, the medium was replaced with PBS containing Hoechst 2 µM for nuclear staining, pre-warmed at 37 °C, which was immediately followed by imaging.

The effect of DMS on cellular G4 prevalence was evaluated by treatment prior to SiR-PyPDS (**1**) labelling: cells were incubated with DMEM containing 20 mM DMS for the indicated times (5, 10 or 20 min). After the desired treatment time, DMS was quenched by adding 10% β-mercapto-ethanol in PBS followed by washing twice with PBS pre-warmed at 37 °C.

Cell-cycle synchronization was performed with mimosine treatment as previously described[5]. Transcriptional and replication arrest was achieved by co-treatment of cells with DRB and aphidicolin, as previously described[18].

Binding of SiR-PyPDS (**1**) to nuclear G4s was visualized using HILO microscopy[15]. The microscope set-up has been described previously[21,22]. The central plane of the nucleus in U2OS cells was found with either bright-field microscopy or using Hoechst staining. For binding event measurements, 400 frames were acquired for each cell with 100-ms exposure time at a power density of 180 W cm^{-2}. For residency time measurements, time lapses of 70 frames were acquired every 3 s with an exposure time of 500 ms and a power density of 180 W cm^{-2}.

Residence time determination. Time lapses for both in vitro and cell measurements were analysed using image processing and TrackMate[20], as described in the previous section. The distribution of residence times was fitted to a single-component exponential decay, to determine the characteristic residence time. This value was corrected for photobleaching as previously described[23]. The photobleaching rate for in vitro experiments was determined to be 0.001 s^{-1}, compared to 0.066 s^{-1} for the off rate. This rate was found by measuring the intensity decay of SiR-PyPDS (**1**) at 30× higher excitation power density, where the photobleaching is much faster than the binding kinetics. This decay was fitted to a single exponential decay and, by assuming a linear relationship between power density and photobleaching, the value could be scaled to the actual power density used in the residence time experiments. The photobleaching rate in cells was determined to be 0.01 s^{-1}, compared to 0.16 s^{-1} for the off rate. This rate was found by fitting the intensity decay of the lysosomal accumulation of SiR-PyPDS (**1**) to a single exponential decay.

Reporting Summary. Further information on research design is available in the Nature Research Reporting Summary linked to this Article.

Data availability

All data generated during this study are included in this published Article and its Supplementary Information.

References

19. Chandradoss, S. D. et al. Surface passivation for single-molecule protein studies. *J. Vis. Exp.* **86**, 50549 (2014).
20. Tinevez, J.-Y. et al. TrackMate: an open and extensible platform for single-particle tracking. *Methods* **115**, 80–90 (2017).
21. Ponjavic, A. et al. Single-molecule light-sheet imaging of suspended T cells. *Biophys. J.* **114**, 2200–2211 (2018).
22. Ponjavic, A., Ye, Y., Laue, E., Lee, S. F. & Klenerman, D. Sensitive light-sheet microscopy in multiwell plates using an AFM cantilever. *Biomed. Opt. Express* **9**, 5863–5880 (2018).
23. Chen, J. et al. Single-molecule dynamics of enhanceosome assembly in embryonic stem cells. *Cell* **156**, 1274–1285 (2014).

Acknowledgements

This work was supported by programme grant funding from Cancer Research UK (C9681/A18618, to S.B.), core funding from Cancer Research UK (C14303/A17197, to S.B.), a Royal Society University Research Fellowship (UF120277, to S.F.L.), a Research Professorship (RP150066, D.K.), the EPSRC (EP/L027631/1, to D.K.) and a BBSRC David Phillips Fellowship (BB/R011605/1, to M.D.A.).

Author contributions

M.D.A., A.P., D.K. and S.B. conceived and designed the experiments. M.D.A. performed the design, synthesis and biophysical characterization of G4 ligands. A.P. developed the microscope and protocols used for imaging. M.D.A., A.P. and R.T.R. performed in vitro imaging experiments. R.T.R. carried out surface preparation for in vitro experiments. M.D.A., A.R. and A.P. performed imaging experiments in cells. A.P. analysed imaging data. M.C., A.R. and X.Z. contributed to the synthesis and biophysical validation of the ligands. M.D.A., A.P., R.T.R., S.F.L., D.K. and S.B. contributed to the study design. J.S. assisted with DMS experiments. A.R. contributed to cellular staining and imaging. A.R. and L.-M.N. characterized the fluorescence properties of the G4 ligands. M.D.A., A.P., D.K. and S.B. interpreted the results and co-wrote the manuscript. All authors discussed the results and commented on the manuscript.

Competing interests

S.B. is a founder and shareholder of Cambridge Epigenetix Ltd.

Additional information

Extended data is available for this paper at https://doi.org/10.1038/s41557-020-0506-4.

Supplementary information is available for this paper at https://doi.org/10.1038/s41557-020-0506-4.

Correspondence and requests for materials should be addressed to D.K. or S.B.

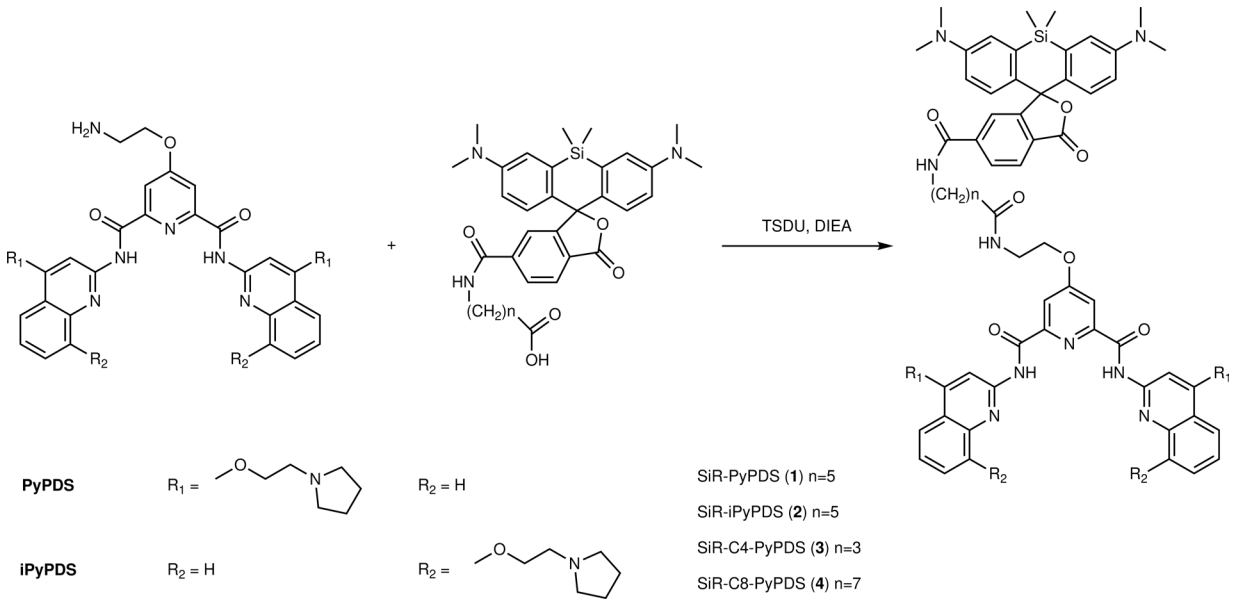

Extended Data Fig. 1 | SiR-PyPDS analogues synthesized. SiR-PyPDS analogues (**1**, **2**, **3** and **4**) with different chemical linkers between the PyPDS and the SiR scaffold synthesised in this study. TSTU was used as amide coupling reagent in the synthesis of all 3 analogues.

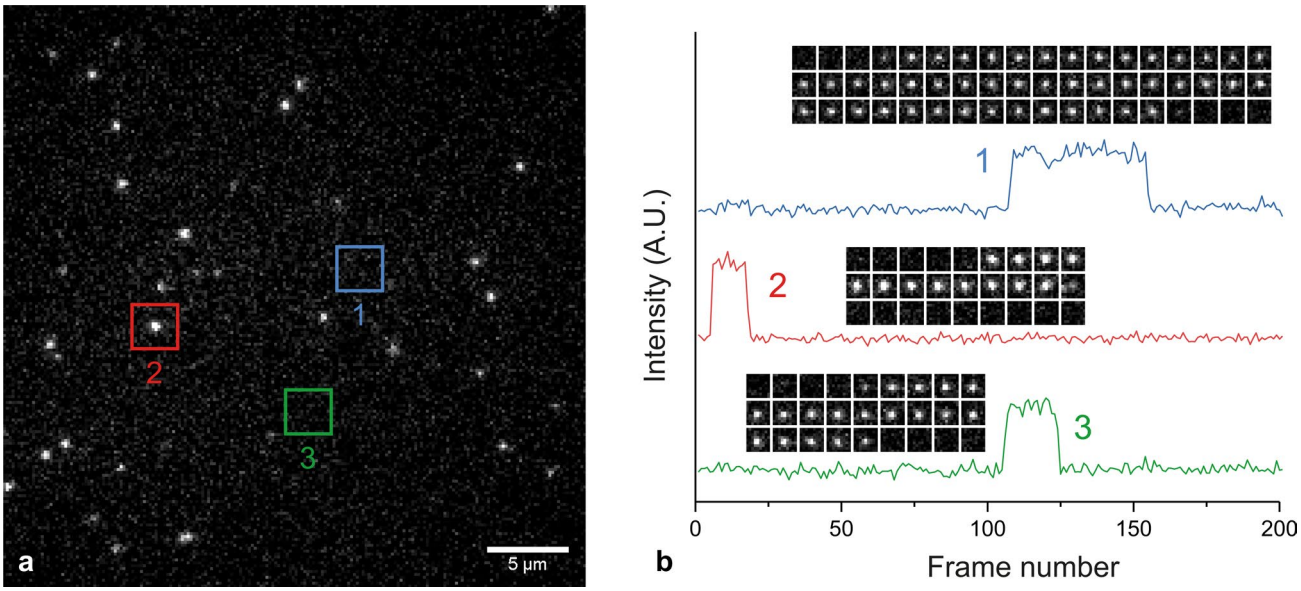

Extended Data Fig. 2 | Single-step photobleaching confirms detection of individual probes. a, 25 pM SiR-PyPDS binding to MYC *in vitro*. The red square indicates a single binding event. **b**, Intensity traces from three binding events in (**a**), showing probes undergoing single-step photobleaching. The insets show time lapses for each molecule. Similar single-step photobleaching could be consistently observed in all single-molecule video acquisitions.

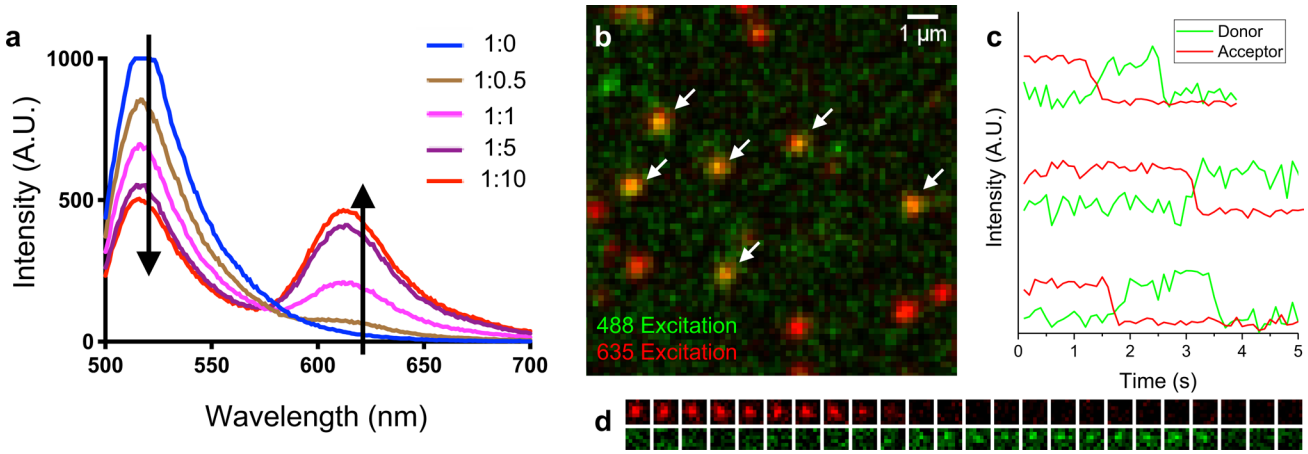

Extended Data Fig. 3 | FRET between SiR-PyPDS and Alexa Fluor 488-labelled MYC confirms direct binding to G4s. a, Emission spectrum of 488-MYC-G4 at 1µM and SiR-PyPDS at various stoichiometric ratios. As the probe concentration increases, donor emission drops and acceptor emission increases, indicating FRET. **b**, *In vitro* G4 FRET experiment. 250 pM of SiR-PyPDS (shown in red with acceptor excitation) interacting with Alexa Fluor 488-labelled MYC-G4 (with ~1% surface coverage). The green channel shows acceptor emission under donor excitation. FRET between MYC and SiR-PyPDS is highlighted with white arrows. **c**, 10 nM SiR-PyPDS interacting with 488-MYC-G4 (0.001% surface coverage). Temporal intensity traces of donor (green) and acceptor (red) emission under donor excitation. Anti-correlated intensity fluctuation upon acceptor photobleaching indicates single-molecule FRET between PyPDS and MYC. **d**, Example time lapse of acceptor (top, red) and donor (bottom, green) emission from (**c**). Experiments a-d were performed as 3 independent replicates all providing similar results.

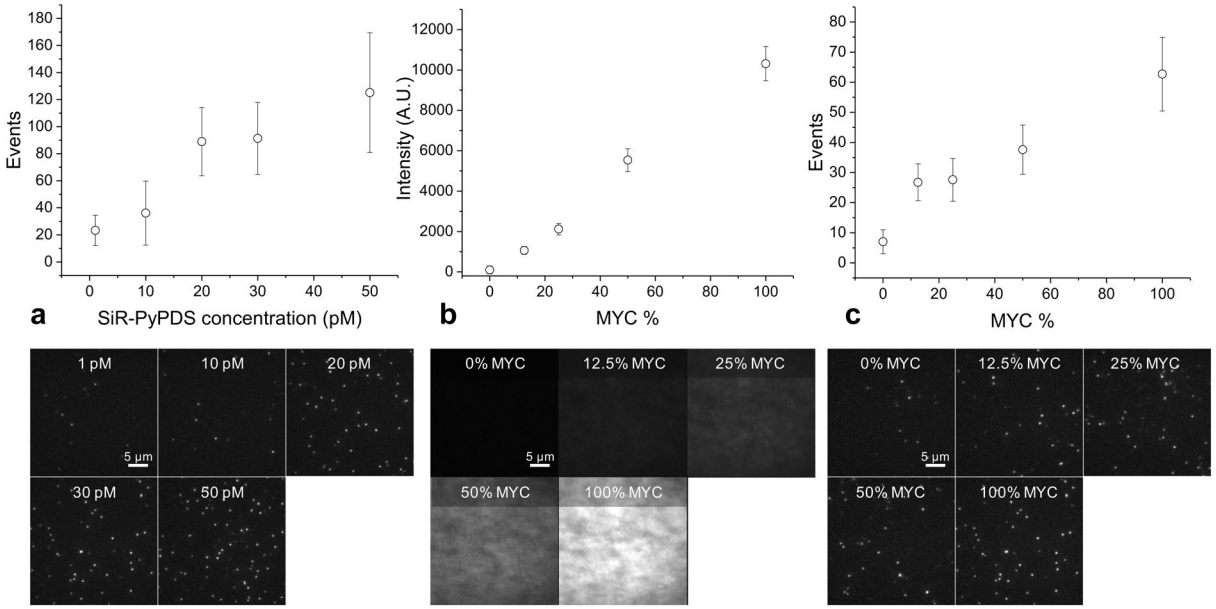

Extended Data Fig. 4 | Single-molecule imaging with SiR-PyPDS can be used to quantify MYC-G4 prevalence *in vitro*. **a**, Number of detected binding events increases with probe concentrations. **b**, MYC fluorescence showing that the concentration of MYC on the surface can be controlled by mixing with a competing biotinylated oligomer. **c**, Number of detected events increases with G4 concentration. Sample images for each condition is shown beneath each plot. Error bars indicate mean ± sd. n=12 measurements taken from 2 independent replicates.

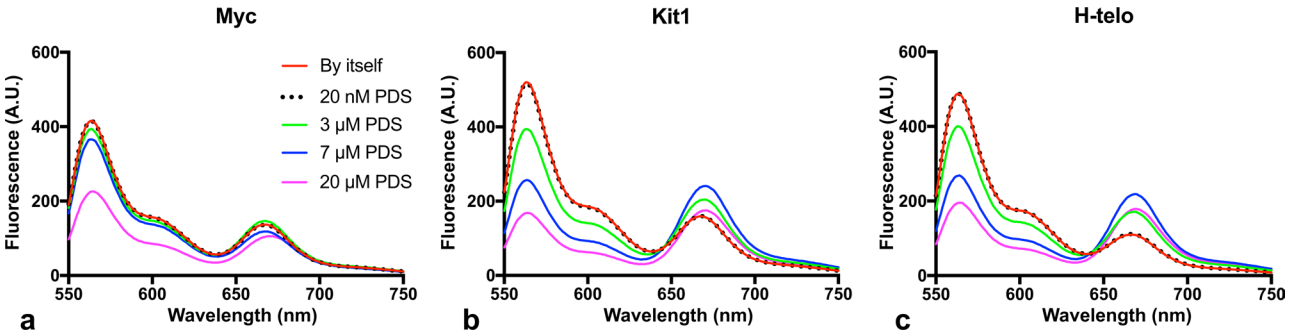

Extended Data Fig. 5 | Induction of G4-folding by increasing concentrations of SiR-PyPDS measured with dually labelled FRET oligos. a-**c**, Fluorescence emission spectra under Cy3 excitation for each G4 sequence. Experiments **a**-**c** were performed as 3 independent replicates all providing similar results.

	H-telo (1 μM) unfolding		c-KIT1 (1 μM) unfolding	
Condition	Slow $t_{1/2}$ / min	Fast $t_{1/2}$ / min	Slow $t_{1/2}$ / min	Fast $t_{1/2}$ / min
No ligand	113.5 ±0.9	11.2 ±0.2	240.6 ±0.7	13.4 ±0.2
SiR-PyPDS 20 nM	125.0 ±0.8	10.0 ±0.1	284.9 ±0.8	14.7 ±0.2
SiR-PyPDS 100 nM	129.3 ±1.1	10.7 ±0.2	282.5 ±0.8	15.2 ±0.2
SiR-PyPDS 1 μM	128.2 ±0.7	8.1 ±0.1	451.6 ±3.0	13.7 ±0.2

Extended Data Fig. 6 | The effect on SiR-PyPDS binding on unfolding kinetics of G4 DNA sequences *in vitro*. G4 two-phase unfolding kinetics were measured by introducing 10 μM of respective complimentary DNA oligonucleotide at t=0 to trap the unfolded G4 oligonucleotide state. Data presented here are of best fit of a two-phase association model. Error indicates the standard error of the fit. n=1 measurement for each condition. Each experiment has been repeated 3 times providing consistent results.

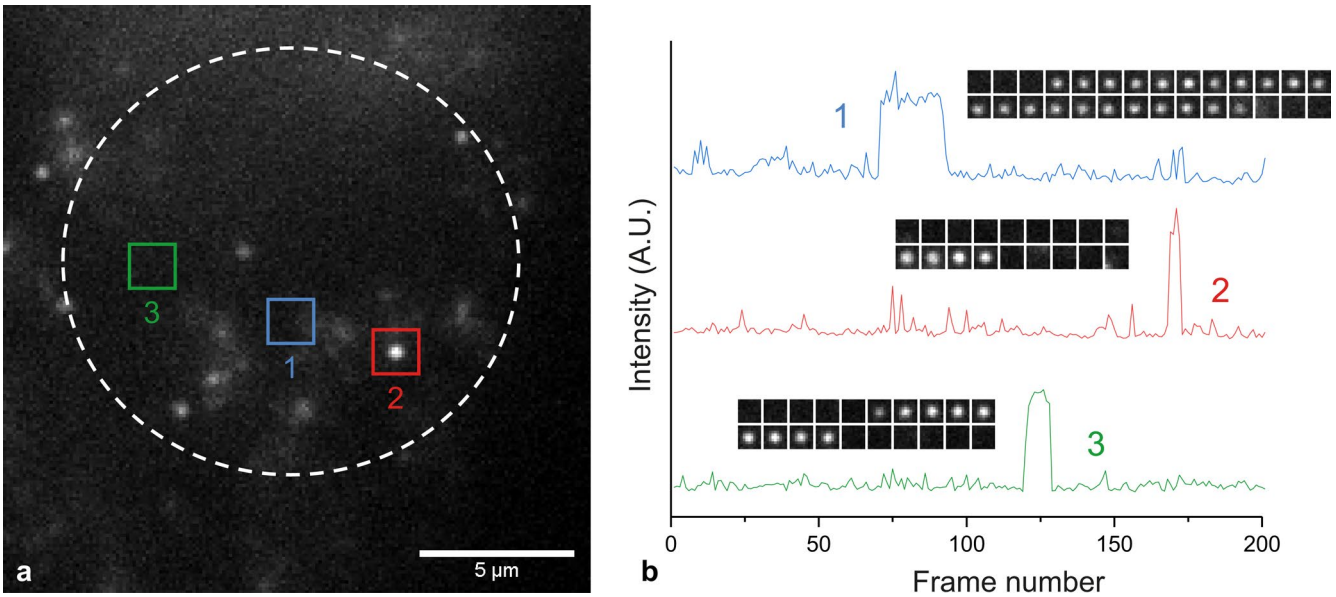

Extended Data Fig. 7 | Single-step photobleaching confirms detection of individual probes in cells. a, 20 nM SiR-PyPDS binding to targets in a living cell. The red square indicates a single binding event. **b**, Intensity traces from three binding events in A, showing probes undergoing single-step photobleaching. The insets show time lapses for each molecule. Similar single-step photobleaching could be observed in all single-molecule video acquisitions.

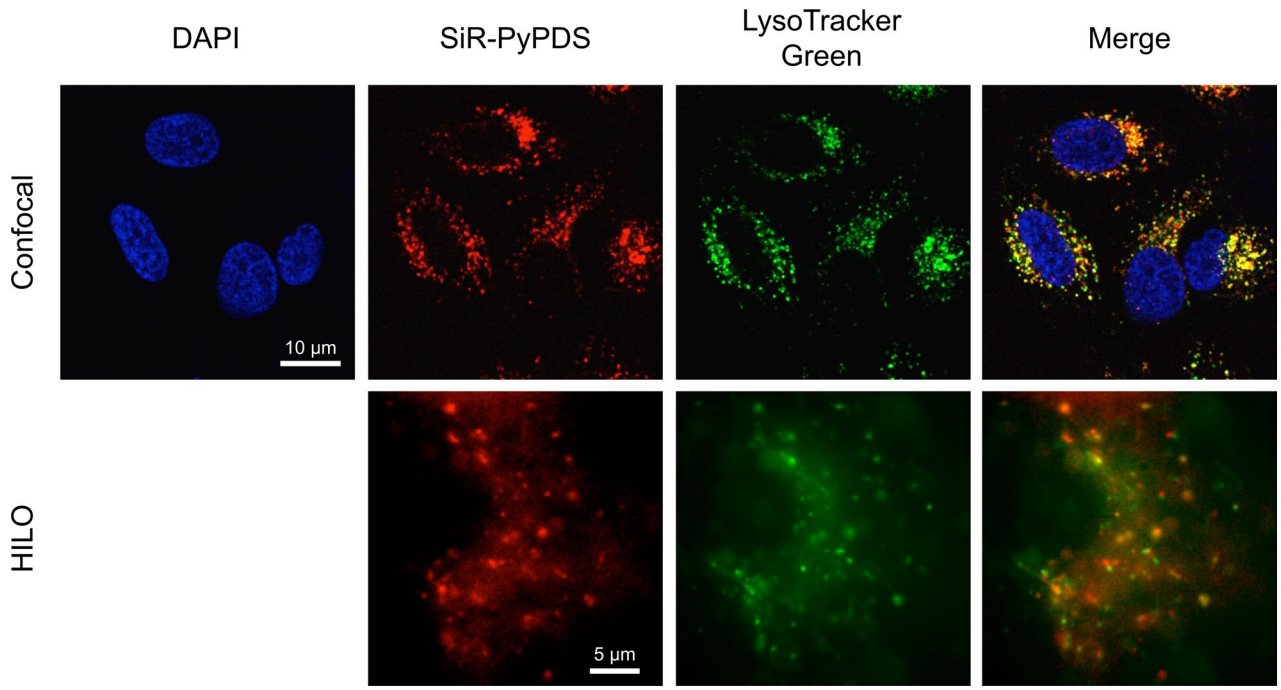

Extended Data Fig. 8 | SiR-PyPDS mainly accumulates in lysosomes. Representative confocal and HILO microscopy images obtained in the presence of SiR-PyPDS (1 µM in confocal and 40 nM in HILO) and LysoTracker Green (50 nM), confirming co-localisation of extra-nuclear staining with lysosomes. Experiments have been repeated 3 times providing similar results.

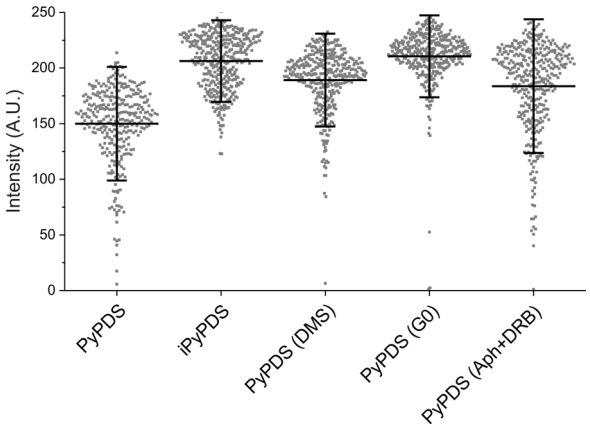

Extended Data Fig. 9 | Total nuclear accumulation of SiR-PyPDS and SiR-iPyPDS in U2OS cells. Total fluorescence intensity measured inside the nuclei of >300 U2OS cells after incubation with 10μM SiR-PyPDS or SiR-iPyPDS by standard confocal microscopy at 633 nm. Each point on the graph represents the total fluorescence of SiR measured at 633 nm per nuclei, data are plotted as the mean of >300 nuclei measured in 3 independent replicates. Total fluorescence measurement revealed comparable ability of the two molecules to accumulate in the nuclei. Error bars indicate mean ± sd.

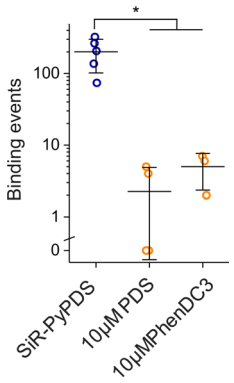

Extended Data Fig. 10 | Cellular displacement experiments of SiR-PyPDS with the established G4-ligands PDS and PhenDC3. Displacement of SiR-PyPDS in cells by competition with 10 μM of unlabelled G4-ligands PDS and PhenDC3. Cells were pre-incubated 30 minutes with PDS or PhenDC3 at 10 μM prior standard single-molecule imaging with SiR-PyPDS. Each point on the graph depicts the number of long-lived SiR-PyPDS event measured in independent replicates. Data are plotted as the mean of 3 or more independent replicates. Error bars indicate mean ± sd. * $P < 0.05$, two-sided Mann–Whitney *U*-test. n = 5,3 and 3 measurements taken from 3 independent replicates for no displacement, PDS displacement and PhenDC3 displacement respectively.

nature research

Corresponding author(s): Shankar Balasubramanian
David Klenerman

Last updated by author(s): 06/05/2020

Reporting Summary

Nature Research wishes to improve the reproducibility of the work that we publish. This form provides structure for consistency and transparency in reporting. For further information on Nature Research policies, see Authors & Referees and the Editorial Policy Checklist.

Statistics

For all statistical analyses, confirm that the following items are present in the figure legend, table legend, main text, or Methods section.

n/a	Confirmed	
☐	☒	The exact sample size (*n*) for each experimental group/condition, given as a discrete number and unit of measurement
☐	☒	A statement on whether measurements were taken from distinct samples or whether the same sample was measured repeatedly
☐	☒	The statistical test(s) used AND whether they are one- or two-sided *Only common tests should be described solely by name; describe more complex techniques in the Methods section.*
☒	☐	A description of all covariates tested
☒	☐	A description of any assumptions or corrections, such as tests of normality and adjustment for multiple comparisons
☐	☒	A full description of the statistical parameters including central tendency (e.g. means) or other basic estimates (e.g. regression coefficient) AND variation (e.g. standard deviation) or associated estimates of uncertainty (e.g. confidence intervals)
☐	☒	For null hypothesis testing, the test statistic (e.g. *F*, *t*, *r*) with confidence intervals, effect sizes, degrees of freedom and *P* value noted *Give P values as exact values whenever suitable.*
☒	☐	For Bayesian analysis, information on the choice of priors and Markov chain Monte Carlo settings
☒	☐	For hierarchical and complex designs, identification of the appropriate level for tests and full reporting of outcomes
☒	☐	Estimates of effect sizes (e.g. Cohen's *d*, Pearson's *r*), indicating how they were calculated

Our web collection on statistics for biologists contains articles on many of the points above.

Software and code

Policy information about availability of computer code

Data collection	Micromanager 1.4, BMG PHERAstar Plus, Cary Eclipse Fluorescence Spectrophotometer, Applied Photo-physics Chirascan circular dichroism spectropolarimeter
Data analysis	ImageJ 1.52, Matlab 2016b, OriginPro 2017, GraphPad Prism 8, Mestrenova, Cary Kinetics

For manuscripts utilizing custom algorithms or software that are central to the research but not yet described in published literature, software must be made available to editors/reviewers. We strongly encourage code deposition in a community repository (e.g. GitHub). See the Nature Research guidelines for submitting code & software for further information.

Data

Policy information about availability of data

All manuscripts must include a data availability statement. This statement should provide the following information, where applicable:

- Accession codes, unique identifiers, or web links for publicly available datasets
- A list of figures that have associated raw data
- A description of any restrictions on data availability

All data are available in the manuscript, supporting information and supporting videos.

Field-specific reporting

Please select the one below that is the best fit for your research. If you are not sure, read the appropriate sections before making your selection.

☒ Life sciences ☐ Behavioural & social sciences ☐ Ecological, evolutionary & environmental sciences

Life sciences study design

All studies must disclose on these points even when the disclosure is negative.

Sample size	A minimum of 2 biological replicates each including a minimum of 3 independent replicates provided consistent and reproducible measurements of binding lifetimes and binding event. Most of the experiments are performed in 3 biological replicated each including a minimum of 5 independent replicates, unless otherwise stated. Further increase of the sample size did not result in any valuable improvement of statistical significance
Data exclusions	No samples were excluded
Replication	All the analysis reported have been performed on a minimum of 2 biological replicates each including a minimum of 3 independent replicates. Most of the experiments are performed in 3 biological replicated each including a minimum of 5 independent replicates, unless otherwise stated. All attempts of replication were successful.
Randomization	Different investigators have repeated and reproduced different experiments.
Blinding	Blinding was not possible as the same investigators were simultaneously preparing the sample and imaging it.

Reporting for specific materials, systems and methods

We require information from authors about some types of materials, experimental systems and methods used in many studies. Here, indicate whether each material, system or method listed is relevant to your study. If you are not sure if a list item applies to your research, read the appropriate section before selecting a response.

Materials & experimental systems

n/a	Involved in the study
☒	☐ Antibodies
☐	☒ Eukaryotic cell lines
☒	☐ Palaeontology
☒	☐ Animals and other organisms
☒	☐ Human research participants
☒	☐ Clinical data

Methods

n/a	Involved in the study
☒	☐ ChIP-seq
☒	☐ Flow cytometry
☒	☐ MRI-based neuroimaging

Eukaryotic cell lines

Policy information about cell lines

Cell line source(s)	U2OS cells were provided by the CRUK, Cambridge Institute Biorepository Core Facility
Authentication	U20S cells were genotype authenticated by the CRUK Cambridge Institute Biorepository Core Facility
Mycoplasma contamination	The cells were tested for mycoplasma contamination prior use and no contamination was detected by RNA-capture ELISA
Commonly misidentified lines (See ICLAC register)	U2OS cell lines